Topology-Inspired Galilean Invariant Vector Field Analysis

Roxana Bujack*
Technical University
Kaiserlautern
Germany

Mario Hlawitschka†
Leipzig University of
Applied Sciences
Germany

Kenneth I. Joy‡
University of
California Davis
USA

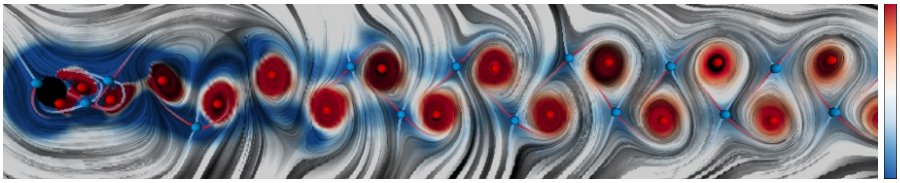

Figure 1: The Galilean invariant vector field and topology in the flow behind a cylinder. Jacobian determinant is encoded in the color map.

ABSTRACT

Vector field topology is one of the most powerful flow visualization tools, because it can break down huge amounts of data into a compact, sparse, and easy to read description with little information loss. It suffers from one main drawback though: The definition of critical points, which is the foundation of vector field topology, is highly dependent on the frame of reference.

In this paper we propose to consider every point as a critical point and locally adjust the frame of reference to the most persistent ones, that means the extrema of the determinant of the Jacobian. The result is not the extraction of one well-suited frame of reference, but the simultaneous visualization of the dominating frames of reference in the different areas of the flow field. Each of them could individually be perceived by an observer traveling along these critical points. We show all important ones at once.

1 INTRODUCTION

The topological skeleton of a flow field consists of its critical points and separatrices, i.e. the positions that have zero velocity and their one-dimensional invariant manifolds. Let $v : \mathbb{R}^2 \times \mathbb{R} \to \mathbb{R}^2$,

$$v(x,t) = \dot{x} = \frac{dx}{dt} = \begin{pmatrix} v_1(x,t) \\ v_2(x,t) \end{pmatrix}, \tag{1}$$

be a two-dimensional vector field describing the instantaneous velocity of a flow. Then, there are three principle types of critical points: saddles, sources, and sinks. Further, there are transitional types, like centers. The categorization of the so called first order critical points is performed using the eigenvalues of the Jacobian, which is the matrix of the first derivatives

$$\nabla v(x,t) = \begin{pmatrix} \frac{\partial v_1(x,t)}{\partial x_1} & \frac{\partial v_1(x,t)}{\partial x_2} \\ \frac{\partial v_2(x,t)}{\partial x_1} & \frac{\partial v_2(x,t)}{\partial x_2} \end{pmatrix}. \tag{2}$$

The different cases, which can be found in Figure 2, can be expressed compactly by means of the determinant of the Jacobian. A negative determinant corresponds to saddle, while a positive determinant corresponds to a source, a sink, or a vortex

$$\begin{aligned} &\det\nabla v(x) < 0 \Leftrightarrow x \text{ is a saddle,} \\ &\det\nabla v(x) > 0 \Leftrightarrow x \text{ is a source, sink, or vortex.} \end{aligned} \tag{3}$$

Only the saddles have one-dimensional invariant manifolds, which are the sets of points that are mapped onto themselves as they move tangentially to the vector field. They are called separatrices and can be calculated by integrating forward and backward in the directions of the eigenvectors of the Jacobian of a saddle critical point.

*e-mail: bujack@ucdavis.edu
†e-mail: mario.hlawitschka@htwk-leipzig.de
‡e-mail: joy@cs.ucdavis.edu

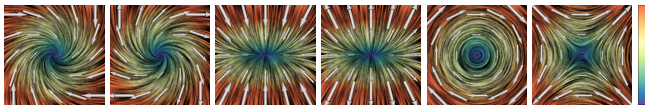

Spiral sink:	Sp. source:	Node sink:	N. source:	Center:	Saddle:
$\Re(\lambda_{1/2}) < 0,$	$\Re(\lambda_{1/2}) > 0,$	$\Re(\lambda_{1/2}) < 0,$	$\Re(\lambda_{1/2}) < 0,$	$\Re(\lambda_{1/2}) = 0,$	$\Re(\lambda_1) > 0,$
$\Im(\lambda_{1/2}) \neq 0.$	$\Im(\lambda_{1/2}) \neq 0.$	$\Im(\lambda_{1/2}) = 0.$	$\Im(\lambda_{1/2}) = 0.$	$\Im(\lambda_{1/2}) \neq 0.$	$\Re(\lambda_2) < 0.$

Figure 2: Classification of the two-dimansional critical points depending on the eigenvalues λ_1, λ_2 of the Jacobian. The colorbar represents the speed.

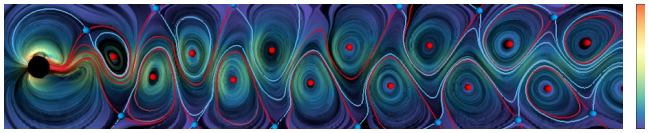

(a) Result with removed average flow.

(b) Result without removed average flow.

Figure 3: Dependence of classical vector field topology on the choice of a suitable frame of reference in the example of a flow behind a cylinder on top of line integral convolution (LIC) [4] with the speed encoded in the colormap from Figure 2.

The topological skeleton separates the flow into regions in which all particles have the same origin and destination. The result is a

highly compressed representation of the vector field that still contains all the important features of the corresponding frame of reference. This property makes vector field topology a very useful tool in flow visualization. An example of the classical vector field topology can be found in Figure 3a. Saddles are drawn in blue and centers are in red. The colors of the separatrices resemble the Doppler effect. As they move away from their aboriginal saddles, they are drawn in red like distancing objects experience a red shift. Analogously, the separatrices we get from backward integration are drawn in blue like in resemblance with the blue shift of approaching objects. But Figure 3b also demonstrates the big drawback of vector field topology. It can only yield meaningful results if the frame of reference was chosen wisely. In some situations all the wisdom in the wold will not solve the problem because there is no ubiquitous frame of reference that allows the simultaneous visualization of all relevant features. It is, for example, not possible to find one single frame that shows the von Kármán vortex street from Figure 3a as well as the first vortex that is forming directly behind the obstacle, which can be seen in Figure 3b.

This problem is long known in flow analysis, but has not yet been solved in a satisfactory way. For example Parry and Tan [25] state: "There does not appear to be any single precisely defined convection velocity which is best for 'viewing' the patterns." and Haller [11]: "There are several natural choices for a frame of reference: the lab frame, the frame co-rotating with the boundary, or the frames co-rotating with individual vortices."

Considering multiple frames of reference is not trivial because every single point in the vector field is a critical point just given the right frame of reference. That means, we have one vector field for every point in the data, which doubles the dimensionality of the problem. To overcome this issue, we will select a subset of particularly persistent points based on Galilean invariant criteria and visualize their frame of reference in their local neighborhood. That way, we can visualize both, the vortex street from Figure 3a and the first vortex behind the obstacle from Figure 3b in just one image, compare Figure 1.

In this paper, we suggest a method that is based on the determinant of the Jacobian because it determines the category of a critical point and is Galilean invariant. That means, even though a point can be a critical point or not depending on the frame of reference, the kind of critical point it would be, is always the same.

Small perturbations in the vector could change the category a critical point falls into if the magnitude of the Jacobian is close to zero. That means the higher the magnitude, the more persistent the potential critical point. That is why we concentrate on the most robust ones by using the extrema of the determinant field as critical point candidates.

In a nutshell, the presented method can be described as follows:

1. Calculate the scalar topology of the determinant of the Jacobian of the vector field.
2. Reduce the number of critical points of the determinant field using contour tree pruning.
3. Construct the Galilean invariant vector field by subtracting a weighted sum of the velocities at the persistent positive maxima and negative minima.
4. Integrate the separatrices in the Galilean invariant vector field.

2 Related Work

Vector field topology is based on the theory of dynamical systems [22], which employs the concepts of critical points and separatrices and goes back to Poincareé [27]. The different flow patterns of vector field critical points categorized by the eigenvalues of their Jacobian into saddles, sinks, sources, and vortices were summarized already by Perry and Chong [23]. Hellman and Hesselink introduced the topology approach to the visualization community [15]. Since then, it has become a crucial component of flow visualization. An overview can be found in the state of the art reports [29, 19] and with an emphasis on unsteady flow in [26].

The problem of finding a good frame of reference for the analysis and visualization of flow fields has been approached in different ways [24, 13]. The probably most intuitive one is to subtract the mean flow of the field. Wiebel et al. [38] show that subtraction of the potential field computed by the Helmholtz-Hodge-decomposition [20, 28] yields more coherent results. This approach is later also followed by Bhatia et al. [2]. Another technique removes the boundary-induced flow at localized areas [9]. The results of these approaches depend on the chosen area and its boundary and are only capable of treating one frame of reference per area.

Fuchs et al. [10] state that there may not be one single frame of reference that is well suited to visualize an unsteady flow field in all time steps, but that the frame of reference may have to change over time. As an indicator for the frame of reference, they use the minima of the acceleration field as suggested by Kasten et al. [18].

In this paper, we go one step further and claim that even in steady fields, there is generally not one perfect frame of reference that allows the absolute analysis of all features. Suitable frames may have only local validity and we have to change the perspective of the observer not only if we move in time, but also if we move in space.

We categorize the points in the vector field not by the properties of their velocity, but their Jacobian. This way, regions with separating characteristics are distinguished from regions with repelling or attracting behavior. A similar segmentation has been used by Theisel et al. for pathline-based topology [33].

3 Coordinate Transformations

In this section, we revisit the behavior of the basic derivatives under coordinate transformations. An introduction to the physical principles can be found, for example, in [21, 30].

We look at a transformation of coordinates $(x,t) \in \mathbb{R}^2 \times \mathbb{R}$ of the form

$$\begin{aligned} x' &= Ax + b, \\ t' &= t + c \end{aligned} \tag{4}$$

with a constant orthogonal matrix $A \in SO(2)$, a time dependent vector $b : \mathbb{R} \to \mathbb{R}^2$, and a constant time shift $c \in \mathbb{R}$.

A Galilean transformation is a subset of (4) with the additional restriction of b depending only linearly on time, $\dot{b} = const$.

A scalar field $s(x,t)$, a vector field $v(x,t)$, and a matrix field $M(x,t)$ are called invariant with respect to a coordinate transformation [32] if they suffice

$$\begin{aligned} s'(x',t') &= s(x,t), \\ v'(x',t') &= Av(x,t), \\ M'(x',t') &= AM(x,t)A^{-1}. \end{aligned} \tag{5}$$

The velocity field

$$v(x,t) = \frac{dx}{dt} = \dot{x} \tag{6}$$

is not invariant under the transformation (4) because it leads to

$$\begin{aligned} \frac{\partial x_i}{\partial x'_j} &= A^{-1}_{ij} \\ \frac{dt}{dt'} &= 1, \end{aligned} \tag{7}$$

and therefore

$$\begin{aligned} v'(x',t') = \frac{dx'}{dt'} = \frac{dx'}{dt}\frac{dt}{dt'} &\overset{(7)}{=} \frac{dx'}{dt} \\ &\overset{(4)}{=} \frac{dAx+b}{dt} = A\dot{x} + \dot{b} \overset{(6)}{=} Av(x,t) + \dot{b}. \end{aligned} \tag{8}$$

That means v is not invariant except for constant displacements $b \in \mathbb{R}$. Especially, it is not Galilean invariant. As a result, the critical points defined as the zeros in the velocity field are not Galilean invariant either.

The Jacobian of a velocity field or the velocity gradient,

$$J(x,t) = \nabla_x v(x,t), \tag{9}$$

on the other hand, is invariant with respect to (4), because from

$$\nabla_{x'} v(x) \overset{(7)}{=} \nabla_x v(x) A^{-1}, \tag{10}$$

follows

$$\begin{aligned} J'(x',t') = \nabla_{x'} v'(x',t') &\overset{(8)}{=} \nabla_{x'}(Av(x,t)+\dot{b}) = A\nabla_{x'} v(x,t) \\ &\overset{(10)}{=} A\nabla_x v(x,t)A^{-1} \overset{(9)}{=} AJ(x,t)A^{-1}. \end{aligned} \tag{11}$$

Especially, the determinant of the Jacobian is invariant because

$$\det J'(x',t') \overset{(11)}{=} \det(AJ(x,t)A^{-1}) = \det J(x,t). \tag{12}$$

4 Galilean Invariant Critical Points

A critical point in the classical definition is a point with vanishing velocity. This property changes depending on the frame of reference because of (8). Especially, for any point $x_0 \in \mathbb{R}^2$, the Galilean transformation with $A = Id, b = -v(x_0,t)t, c = 0$ in (4), i.e. $x' = x - v(x_0,t)t$ converts any x_0 into a critical point, because of

$$v'(x_0',t') \overset{(8)}{=} v(x_0,t) - v(x_0,t) = 0. \tag{13}$$

We will call the corresponding frame of reference $x' = x - v(x_0,t)t$ the frame of reference of x_0 because this would be the perspective of an observer that traveled sitting on the particle at (x_0,t).

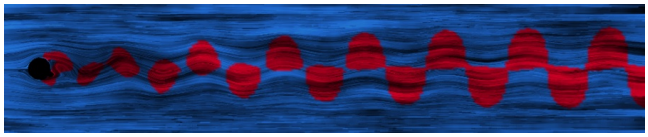

Figure 4: Regions with separating character (negative determinant) shown in blue and regions with attracting/repelling character (positive determinant) shown in red.

In contrast to whether or not a point is a critical point, the category in which a point falls if it is observed from its own frame of reference does not change because of (11). As a result, we can partition each vector field into areas forming saddles (separators) and areas forming sources, sinks, or vortices (attractors/repellers) in their own frame of reference by distinguishing the parts with negative determinant of the Jacobian from positive ones. This partition is Galilean invariant. An example can be found in Figure 4.

At the border between two adjacent areas of opposite signs, the determinant is zero. This means that the points with a low determinant magnitude are not very determined in whether they would be a saddle or not in their frame of reference. A small perturbation of the flow could change the category they fall into. The other way around, points that have a high determinant magnitude are very robust in the type of critical point they form in their own frame of reference. This gives rise to the following definition.

Definition 1. *A point $(x_0,t_0) \in \mathbb{R}^2 \times \mathbb{R}$ is a* **Galilean invariant critical point (GICP)** *of a vector field $v : \mathbb{R}^2 \times \mathbb{R} \to \mathbb{R}^2$ if it is a critical point of the determinant of the Jacobian, i.e.*

$$\nabla \det \nabla v(x_0,t_0) = 0. \tag{14}$$

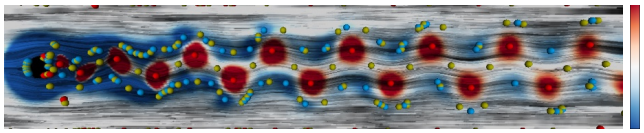

Figure 5: The critical points of the determinant field are color coded in red for maxima, blue for minima, and yellow for saddle points. The color in the LIC encodes the value of the Jacobian determinant.

This definition enables us to use all the well-established tools of scalar topology for the analysis and processing of vector fields.

A scalar field $s : \mathbb{R} \times \mathbb{R} \to \mathbb{R}$ has three different kinds of critical points $\nabla s(x_0,t_0) = 0$: maxima, minima, and saddles. They can be distinguished by the Hessian matrix H_s containing the second spatial derivatives

$$\begin{aligned} H_s(x_0,t_0) \text{ positive definite} &\Leftrightarrow (x_0,t_0) \text{ is a minimum,} \\ H_s(x_0,t_0) \text{ negative definite} &\Leftrightarrow (x_0,t_0) \text{ is a maximum,} \\ H_s(x_0,t_0) \text{ not definite} &\Leftrightarrow (x_0,t_0) \text{ is a saddle.} \end{aligned} \tag{15}$$

The critical points of the determinant field of the Jacobian can be found in Figure 5.

Since we are interested in the points that are very determined in the kind of critical point they form in their own frame of reference, we restrict Definition 1 to the negative minima and the positive maxima. The negative minima of the determinant field form the GI separators, which means the points that form saddles in the velocity field in one specific frame of reference. The positive maxima of the determinant field form the GI attractors and repellers, which means the points that are sources, sinks, and vortices of the velocity field in the respective frame of reference. In the following figures, we visualize the separators using blue and the attractors/repellers using red nodes as it is customary to visualize their analoga in scalar topology. All in all, that leaves us with the following two kinds of interesting Galilean invariant critical points.

Definition 2. *A Galilean invariant critical point $(x_0,t_0) \in \mathbb{R}^2 \times \mathbb{R}$ of a vector field $v : \mathbb{R}^2 \times \mathbb{R} \to \mathbb{R}^2$ is called a* **Galilean invariant separator** *if it suffices*

$$\det \nabla v(x_0,t_0) < 0 \wedge H_{\det \nabla v}(x_0,t_0) \text{ positive definite}, \tag{16}$$

and a **Galilean invariant attractor/repeller** *if it suffices*

$$\det \nabla v(x_0,t_0) > 0 \wedge H_{\det \nabla v}(x_0,t_0) \text{ negative definite}. \tag{17}$$

Theorem 1. *Let (x_0,t_0) be a Galilean invariant separator or attractor/repeller of a velocity field $v : \mathbb{R}^2 \times \mathbb{R} \to \mathbb{R}^2$, then its transformed point (x_0',t_0') under (4) is a Galilean invariant critical point of the same kind in the velocity field $v' : \mathbb{R}^2 \times \mathbb{R} \to \mathbb{R}^2$.*

Proof. The assertion follows directly from (12). □

5 Galilean Invariant Vector Field

The Galilean invariant critical points in general do not coincide with the classical critical points of positions with vanishing velocity. Each of them comes with a frame of reference though in which it becomes a classical critical point. Flow analysts are used to the appearance of the classical critical points as in Figure 2, which is very intuitive. Therefore, we would like to assume the frame of reference of a Galilean invariant critical point to visualize it, so that separators look like saddles and attractors/repellers look like sources, sinks, or vortices respectively. For each GICP, there is a

Galilean transformation that converts us, the observer, into its inherent frame, but there is not one single frame of reference that suffices this claim for all of them.

One possible solution to visualize each GICP in its frame of reference would be an interactive tool with which the user can switch through the different GICPs and their corresponding frames. But there may be many critical points each of the corresponding images would most likely not reveal any significant insight at the areas further away from the selected position. That means we would waste a lot of image space on less relevant information and increase the dimensionality of the problem, because the user would have to dig his way through the vector field actively visiting every GICP.

This is why we follow a different approach. We will construct a derived vector field that locally assumes the inherent frames of references of each GICP. That way, all their frames of reference can be displayed simultaneously without doubling the dimensionality of the problem. We suggest to subtract a weighted average of the velocities of the Galilean invariant separators and attractors/repellers $x_1,...,x_n$ of the vector field v. Any linear interpolation problem

$$\sum_{i=1}^{n} w_i(x) f(x_i) \tag{18}$$

with weights $w_i : \mathbb{R}^2 \to \mathbb{R}, x \mapsto w_i(x)$ that are invariant under (4)

$$w_i'(x') = w_i(x) \tag{19}$$

and add up to one

$$\forall x \in \mathbb{R}^2 : \sum_{i=1}^{n} w_i(x) = 1 \tag{20}$$

will result in a frame of reference independent vector field. Most popular interpolation schemes satisfy these claims, like for example, constant, barycentric, bilinear, or inverse distance interpolation. The weighting sum approach has already been successfully applied to the design of vector fields from user-specified features [35, 39, 8]. For the images in this paper, we use the inverse distance weighting with exponent $p = 2$.

Definition 3. *Let $v : \mathbb{R}^2 \times \mathbb{R} \to \mathbb{R}^2$ be a vector field, $x_1, \ldots, x_n \in \mathbb{R}^2$ a set of points, and w_i the weights of a linear interpolation problem sufficing* (19) *and* (20)*. Then, the* **Galilean invariant vector field (GIVF)** *$\bar{v} : \mathbb{R}^2 \times \mathbb{R} \to \mathbb{R}^2$ is defined by*

$$\bar{v}(x) := v(x) - \sum_{i=1}^{n} w_i(x) v(x_i). \tag{21}$$

Theorem 2. *The Galilean invariant vector field $\bar{v} : \mathbb{R}^2 \times \mathbb{R} \to \mathbb{R}^2$ from Definition 3 is invariant with respect to transformations of the form* (4)*.*

Proof. The assertion follows from straight calculation

$$\begin{aligned}
\bar{v'}(x') &\overset{(21)}{=} v'(x') - \sum_{i=1}^{n} w_i'(x') v'(x_i') \\
&\overset{(19)}{=} v'(x') - \sum_{i=1}^{n} w_i(x) v'(x_i') \\
&\overset{(8)}{=} Av(x)A^{-1} + \dot{b} - \sum_{i=1}^{n} w_i(x)(Av(x_i)A^{-1} + \dot{b}) \\
&\overset{(20)}{=} Av(x)A^{-1} + \dot{b} - \sum_{i=1}^{n} w_i(x) Av(x_i)A^{-1} - \dot{b} \\
&\overset{(21)}{=} A\bar{v}(x)A^{-1},
\end{aligned} \tag{22}$$

and (5). □

Please note that we have proved invariance not only with respect to Galilean transformations, but the more general case of transformations of the form (4). This setting allows a displacement vector b that changes arbitrarily in time. That way, we can trace critical points on their individual paths.

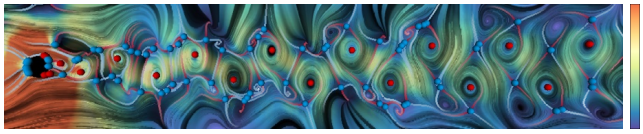

Figure 6: LIC [4] of the GIVF with the GICPs and the speed encoded in the colormap.

A visualization of the frame of reference independent vector field can be found in Figure 6. The Galilean invariant vector field is a normal vector field and can therefore be visualized with any vector field visualization technique independently from showing the determinant, the critical points, or the separatrices.

6 Separatrices

Once, we have chosen a GIVF, we can use it to integrate separatrices. In the classical vector field topology, separatrices are integrated forward and backward along the direction of the eigenvectors of the Jacobian of the saddles until they end at a sink or leave the domain. Since the GIVF has a well defined meaning only within the areas close to the GICPs, we keep integrating the separatrices only for a finite time. For the visualization of this local character, we let them fade out as they leave their origin. Heuristically, a trajectory length of about $1/4$-th of the spacial extent of the domain seemed to yield good results. As before, we encode the direction of integration time in red for distancing and blue for approaching separatrices in analogy with the Doppler effect, compare Figure 7.

7 Topology Based Simplification

As can be seen in Figure 6, in the presence of noise or non smooth fields, many local extrema may appear next to each other, which disturbs the image with a lot of unimportant clutter. This fact is also true for the classical definition of critical points and has led to a whole branch of research on topological simplification [34, 36, 19, 13, 31]. The usual approach is to cancel out close critical points that have indices adding up to zero. This can not trivially be translated to our setting, because we mainly face the repetitive occurrence of GICPs of the same type, which follows from the fact that the saddles in the determinant field have no equivalent in the vector field but we can still use the topological structure of the determinant field to topologically simplify the GIVF.

From now on, we take a closer look at a fixed time $t_0 \in \mathbb{R}$ and skip it from the notation for the sake of brevity. We have seen in (12) that the scalar determinant field of the Jacobian $\det \nabla v : \mathbb{R}^2 \to \mathbb{R}$ is invariant with respect to transforms of the form (4). That means that all operations that we perform using only information from the Jacobian, are invariant in the same sense.

Definition 1 allows us to directly apply scalar topology to vector fields. We will especially make use of the contour tree. We recommend [5, 6] for an introduction to scalar topology simplification.

A contour of a scalar field $f : \mathbb{R}^2 \to \mathbb{R}$ is a connected component of a level set $L_f(h) = \{x \in \mathbb{R}^2, f(x) = h\}$. For increasing $h \in \mathbb{R}$, contours can emerge at local minima of f, join and split at saddles, and disappear at local maxima of f. The contour tree is an abstraction of the scalar field that is formed from shrinking each contour to a node in the tree. Each branch starts and ends at an extremum or a saddle and corresponds to a connected component in the domain.

There are three common measures of importance associated with a branch in the contour tree: persistence, volume, and hypervol-

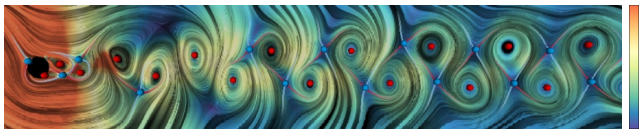

Figure 7: The GIVF from Figure 6 after pruning w.r.t. volume.

ume, [6, 14]. In order to get a vivid understanding of these qualities, imagine that the scalar field describes the height of a mountain range over a two-dimensional map. Persistence is the maximal difference of the scalar values of the components of a branch, i.e. the drop in height from the mountain peak to the closest valley. The volume is the integral over its affiliated points, i.e. the spacial extent of the mountain in the map. Finally, the hypervolume criterion is the integral over the scalar values, i.e. the entirety of material the mountain consists of. Carr et al. [6] use these criteria to simplify the contour tree by pruning branches that do not exceed given thresholds in persistence, volume, or hypervolume. Pruning a branch can be interpreted as an action on the scalar field. Assume we have a branch enclosed by a maximum and a saddle that corresponds to a little mountain that gets pruned. Then, the points in the domain get affiliated with a different branch, namely the one they would belong to if the little mountain was chopped off at the height of the saddle.

Pruning the contour tree of the determinant field, immediately translates to a simplification of the GIVF. The measures persistence, volume, hypervolume, and the affiliation of a point with a branch before and after pruning in a contour tree depend only on the properties of the underlying scalar field. Because of (12), the contour trees of the determinant fields of the Jacobian of two vector fields that differ by a coordinate transform (4) are isomorphous. That means two points x and y are in the same contour, iff x' and y' are in the same contour and if x and y are in adjacent contours in the contour tree, so are x' and y'. The result of pruning with respect to volume in the flow behind a cylinder can be found in Figure 7.

8 Galilean Invariant Clustering

In classical vector field topology, the separatrices segment the domain into regions of similar behavior. Even though a similar segmentation is possible in the GIVF, it lacks an interpretation because of the changing frame of reference in the image. As an alternative, we propose to segment the domain into regions associated with the Galilean invariant critical points.

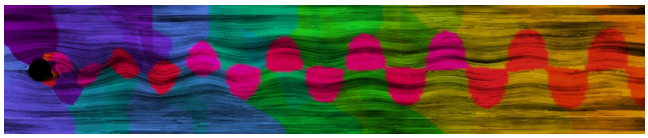

Figure 8: The clustering with respect to steepest ascend/descend for the example of the flow behind a cylinder.

Let $x_1,...,x_n$ be the set of all Galilean invariant separators and attractors/repellers, i.e. the points satisfying Definition 2. Then, we form a cluster for every one of them $C_1,...,C_n$. From each potential separator x_0, i.e. $\det\nabla v(x_0) < 0$, we take the path of the steepest descend until we reach a Galilean invariant separator x_i and assign x_0 to its corresponding cluster C_i. Analogously, for a potential attractor/repeller x_0, i.e. $\det\nabla v(x_0) > 0$, the path of steepest ascend assigns it to its cluster. The paths of the steepest descend/ascend are the integral curves in the potential field $\pm\nabla\det\nabla v(x)$. Therefore it follows from (12) that the resulting segmentation clusters the field into regions of similar behavior that is invariant with respect to (4). An example can be found in Figure 8. This segmentation separates areas of attracting/repelling behavior from areas of separating behavior. Further, each cluster combines all the points that would reveal the same critical point category under a Galilean transformation. That means, assume, we have a point with vanishing velocity that forms a vortex in a flow field. Adding a small constant velocity to the field, will slightly move the center of the vortex. If we add a constant velocity that is big enough, we may be able to make the point of vanishing velocity shift away so far that it will no longer have vortical behavior. This limit, when the type of the point changes, forms the boundary of the associated cluster.

Theorem 3. *Let x_0 be assigned to the cluster C_i associated with the Galilean invariant critical point x_i of a velocity field v, let $x' = Ax + b$ be a coordinate transformation of the form* (4)*, then, the point x_0' is assigned to the cluster C_i' associated with the Galilean invariant critical point x_i' of a velocity field v'.*

Proof. We know from Theorem 1 that (4) maps x_i to x_i' and from (12) that the determinant at all four points $x_0, x_0', x_i x_i'$ has the same sign. The path of steepest descend/ascend from
$p : [0,1] \to \mathbb{R}^2, p(0) = x_0, p(1) = x_i, \frac{dp(s)}{ds} = \pm\nabla\det\nabla v(p(s))$
depends only on the determinant field and therefore inherits the Galilean invariance from (12). That means the transformed path p' is the path of steepest descend/ascend connecting $p'(0) = x_0'$ and $p'(1) = x_i'$, which proves the assertion. □

If two branches in the contour tree get merged during pruning, we also merge the clusters of their corresponding GICP. Let us revisit the mental image of the mountain range. Merging two clusters would correspond to building a bridge between the two mountain tops so that the path of steepest ascend can go on to the highest of the two peaks. Since, the pruning is invariant with respect to (4), the clustering of the field with pruning is also invariant.

9 Case Study

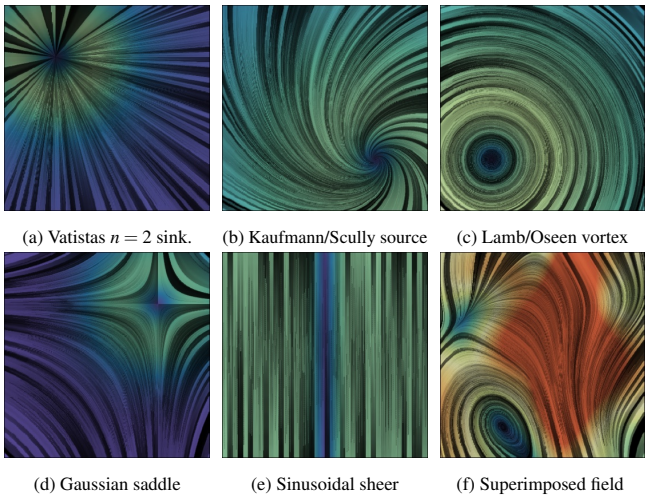

(a) Vatistas $n = 2$ sink. (b) Kaufmann/Scully source (c) Lamb/Oseen vortex

(d) Gaussian saddle (e) Sinusoidal sheer (f) Superimposed field

Figure 9: LIC [4] of the analytic field in Figure 9f, which is the result of superposition of the five other fields.

We have designed an analytic vector field to test our algorithm. It contains four standard flow features (sink, spiral source, center, saddle) each showing a different common velocity profile (Vatistas with $n = 2$, Kaufmann/Scully, Lamb/Oseen, Gaussian, [1, 9]) overlaid with a sheer flow that makes it impossible to view them simultaneously. The single components and their superposition are visualized in Figure 9. They suffice the following mathematical

formulae

$$
\begin{aligned}
v_a(x,y) &= -\frac{1}{\sqrt{1+((x+1)^2+(y-1)^2)^2}}\begin{pmatrix}x+1\\y-1\end{pmatrix},\\
v_b(x,y) &= \frac{\sqrt{0.5}}{1+(x-1)^2+(y+1)^2}\begin{pmatrix}(x-1)+(y+1)\\(y+1)-(x-1)\end{pmatrix},\\
v_c(x,y) &= \frac{1-e^{-(x+1)^2-(y+1)^2}}{(x+1)^2+(y+1)^2}\begin{pmatrix}-(y+1)\\x+1\end{pmatrix},\\
v_d(x,y) &= e^{-(x-1)^2-(y-1)^2}\begin{pmatrix}-(x-1)\\y-1\end{pmatrix},\\
v_e(x,y) &= \begin{pmatrix}0\\1\end{pmatrix}\begin{cases}-0.5, & x<-0.5,\\0.5, & x>0.5,\\\sin(\pi x), & \text{else},\end{cases}\\
v_f(x,y) &= v_a(x,y)+v_b(x,y)+v_c(x,y)+v_d(x,y)+v_e(x,y).
\end{aligned}
\tag{23}
$$

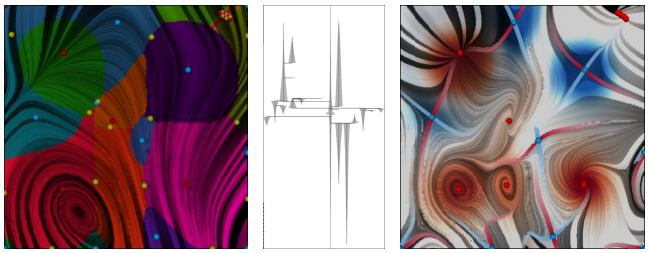

(a) Color map of the clustering, LIC of the analytic field, and the CPs of the determinant field.

(b) Contour tree of the Jacobian determinant.

(c) Color map of the determinant, LIC of the GIVF, and the GI topological skeleton.

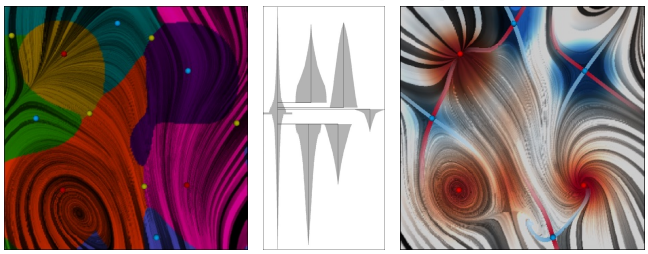

(d) Color map of the clustering, LIC of the analytic field, and the CPs of the determinant field.

(e) Contour tree of the Jacobian determinant.

(f) Color map of the determinant, LIC of the GIVF, and the GI topological skeleton.

Figure 10: Top row without pruning, bottom row after pruning with respect to hypervolume up to a threshold of 200.

Figure 10 shows the result of the Galilean invariant topology without topological simplification in the top row and after pruning with respect to a hypervolume threshold of 200 in the bottom row. The Galilean invariant vector field reveals all the components from Figure 9 and their inherent properties. Superimposing the different components causes them to influence each other a little. For example, the drop of the sheer near the center produces a second center core and additional saddles appear separating the purposefully placed flow features. The additional center core is easily removed using the topological simplification, as can be seen in the bottom row. The additional saddles are inherent in the structure of the vector field. The contour tree is visualized using the algorithm of Heine et al. [14].

Another degree of freedom is the choice of the GIVF. Depending on how we assume the local frames of references, the separatrices look different, compare Figure 11. Increasing the exponent in the inverse distance weighting causes a more local influence the GICP, while lower exponents increase the smoothness of the GIVF. Especially for ∞, the weighting coincides with the nearest neighbor

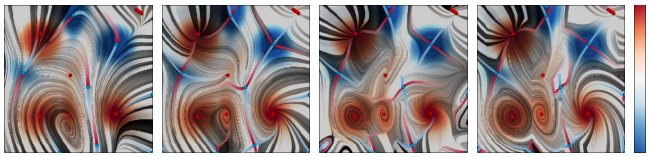

Figure 11: GIVFs without pruning for exponents 0, 1, 4, and ∞ in the inverse distance weighting. The color shows the determinant.

interpolation scheme, which makes the vector field change abruptly at the borders of the Voronoi cells. The other extreme with zero as the exponent leads to a single frame of reference averaged from all GICPs. Depending on the weights, the GIVFs differ and may contain positions that have zero velocity but are no GICPs. For example the classical saddle in the bottom of Figure 10f, which is visually undesirable. Finding the optimal interpolation scheme is outside the scope of this paper. We would like to emphasize that Theorem 2 guarantees Galilean invariance for any of these GIVF.

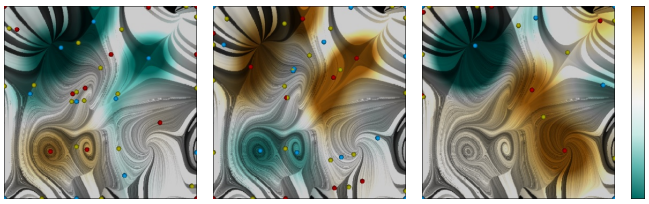

(a) Q-criterion. (b) λ_2-criterion. (c) Divergence.

Figure 12: LIC of the GIVF color coded with respect to popular detectors of vortices and sources/sinks shows their correlation. The nodes are the critical points of the criterium fields. Maxima are red, minima are blue and saddle points are yellow.

The locations of the GICPs do not coincide exactly with the positions where we have placed the centers of the six common flow features in Figure 9. The reason is not that our algorithm does not find them correctly but that the features slightly influence each other due to the superposition. To prove this statement, we use the well established vortex detectors: the Q-criterion [16] and the λ_2-criterion [17] on the original analytic vector field from (23) and show that their results perfectly agree with ours for the location of the vortex core in Figure 12. We have color coded the LIC of the GIVF with the intensity of the different criteria. Figure 12c shows that the sink and the source also perfectly coincide with the minimum and the maximum of the divergence of the original field. Please note that all three criteria are Galilean invariant and therefore would give the same result if applied to the GIVF instead of the original field. Further, the default frame of reference in Figure 9f shows a vortex at the bottom in the middle that is not considered a vortex by the three other methods. We would like to mention that the similarity of the GICP and the extrema of Q, λ_2, and divergence is not surprising, because they are all based on the Jacobian, but this fact does not mean that they are less trustworthy.

10 Results

We applied Galilean invariant vector field topology to some well-known vector field data sets. The results enable us to look at old friends from a new perspective.

Figure 1 shows not only the von Kármán vortex street that forms in the flow behind a cylinder but also the vortices that appear directly at the obstacle. They actually have a much higher vorticity than the distant ones, which is an argument against the usual perspective in Figure 3a, because that does not show these most persistent features.

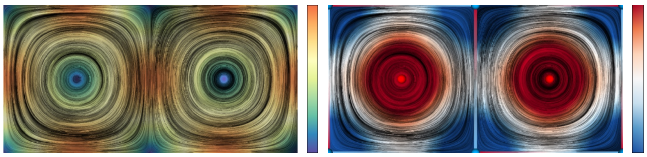

(a) LIC of the original field with speed in the color coding at time $t = 0$.

(b) GIVF and GI topology with the determinant in the color coding, $t = 0$.

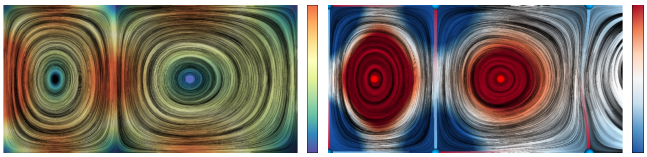

(c) LIC of the original field with speed in the color coding at time $t = 7.5$.

(d) GIVF and GI topology with the determinant in the color coding, $t = 7.5$.

Figure 13: Top row shows the first time step, bottom row the time step of maximal displacement of the double gyre dataset.

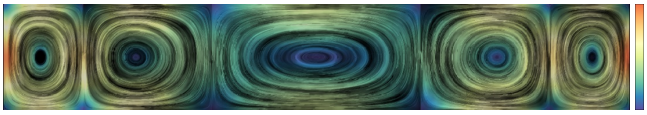

(a) LIC of the original field. The speed is encoded in the color map.

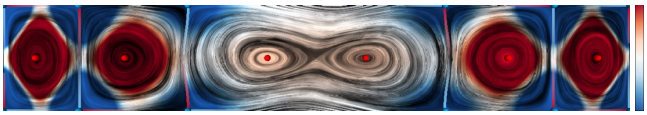

(b) GIVF and GI topology. The Jacobian determinant is encoded in the color map.

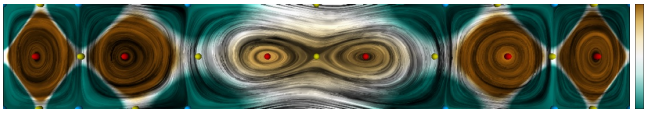

(c) The Q-criterion is encoded in the color map and its critical points in the nodes.

Figure 14: Longer sequence of the double gyre dataset.

Figure 13 shows the double gyre vector field. Its formula can be found in [3]. In our experiments, we use the parameters $A = 0.3\varepsilon = 0.25, \omega = \frac{1}{10}$. The domain $[0,2] \times [0,1]$ shows one pair of infinitely repeating occurrences of gyres. The double gyre is very smooth and no pruning was necessary to create the images. In the first time step, the GIVF coincides with the standard frame of reference because the locations with maximal and minimal determinant of the Jacobian coincide with the classical critical points of vanishing velocity. At all other time steps, this is not the case though. The bottom row of Figure 13 shows the point of maximal displacement. Here, the points of maximal separation do no longer coincide with the positions of vanishing velocity. In their inherent frame of reference, the neighboring gyre from the right starts to enter into the observed domain. In order to give a better explanation of this unusual phenomenon, we have extended the observation domain to $[0,6] \times [0,1]$ in Figure 14. While the standard frame of reference shows one vortex at $(3,0.5)^T$, the GIVF shows two, which is in better accordance with the Q-criterion. The double gyre dataset is a standard example of the analysis of FTLE [12] and a counter example for the validity of classical vector field topology. Please note that the GI separators do not coincide with the FTLE extrema because our method is instantaneous. It works on one time step at a time and does not contain any information about the future path of a particle. Still, there seems to be a relation, whose analysis will be a challenge for future work.

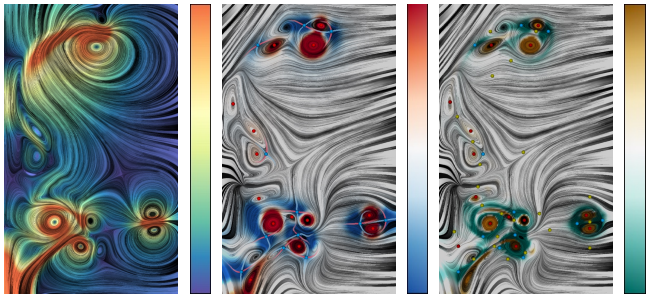

(a) LIC of the original field with speed in the color coding.

(b) GIVF and GI topology with the determinant color coded.

(c) GIVF with the Q-criterion in the color map and its CP.

Figure 15: The swirling jet entering a fluid at rest.

A flow simulation of a swirling jet entering a fluid at rest can be found in Figure 15. The GIVF was pruned with respect to volume up to a threshold of 100. The images show that the default frame of reference is already pretty good. It only misses a few vortices. A very persistent one, for example, at the top of the domain is revealed by the GIVF. This result coincides with the ones of the Q-criterion. The one at the bottom, where the stream enters the domain is a little displaced from the maximum of the two vortex criteria. They place the extremum a bit lower outside the observed domain.

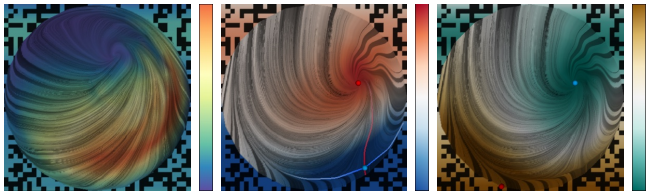

(a) Original field with speed in color coding.

(b) GIVF and topology with the determinant.

(c) For comparison: GIVF with divergence.

Figure 16: The petri dish-data set.

One very challenging flow field [7, 37], which is considered not solved [10, 2] is the petri-dish data set. It contains a spiraling sink that rotates around the center of the circular domain. The result of our approach can be found in Figure 16. We pruned the GIVF with respect to hypervolume at a threshold of 0.001. The position of the sink in the default frame of reference and the GIVF clearly differ. To underline the meaningfulness of the GIVF, we colored the background representing the divergence of the original field in Figure 16c. The maximal divergence coincides with the GI attractor.

Our method can also be applied to different time steps in time-dependent datasets. Some results can be found in the supplementary video. So far, the GIVF does not change smoothly through time. This issue of tracking the critical points is a task for future work.

11 Discussion and Conclusions

In this paper, we have presented a definition of critical points of a vector field that is Galilean invariant based on the extrema of the determinant of the Jacobian. We presented a way to visualize these critical points in an easy to interpret way by means of the Galilean invariant vector field (GIVF). We have proven the invariance and shown the usefulness of the new perspective by presenting insights into popular example vector fields that exceed the features that can be revealed by any single frame of reference.

A drawback of our technique is that the analyst may be tempted to interpret the image as one frame of reference even though it is

the union of many. An interactive tool that switches through the different frames could prevent that from happening. We would also like to mention that in case that a distinguished frame of reference is known to be significant, it may be better to stick with it in contrast to applying our method. Another issue is the dependence of the scalar topological simplification on the choice of the parameters, which our method inherits.

We would like to conclude that not only the vector field topology, but most flow visualization techniques depend sensitively on the chosen frame of reference. The visualization of the Galilean invariant vector field with any visualization technique can aid the analysis of the original vector field.

In our future work, we would like to extend our approach to 3D vector fields and affine transformations and employ feature tracking methods for a smoother handling of time-depending data sets.

Acknowledgments

We would like to thank the FAnToM development group from Leipzig University for providing the environment for the visualization of the presented work. Further, we thank Professor Wolfgang Kollman, Dr. Reymond Chan, and Professor Angela Stevens for providing the datasets used in this publication.

References

[1] M. J. Bhagwat and J. G. Leishman. Correlation of helicopter rotor tip vortex measurements. *AIAA journal*, 38(2):301–308, 2000.

[2] H. Bhatia, V. Pascucci, R. Kirby, and P.-T. Bremer. Extracting Features from Time-Dependent Vector Fields Using Internal Reference Frames. In *Computer Graphics Forum*, volume 33, pages 21–30. Wiley Online Library, 2014.

[3] R. Bujack and K. I. Joy. Lagrangian Representations of Flow Fields with Parameter Curves. In *Large Data Analysis and Visualization (LDAV), 2015 IEEE 4th Symposium on*. IEEE, 2015.

[4] B. Cabral and L. C. Leedom. Imaging vector fields using line integral convolution. In *Proceedings of the 20th annual conference on Computer graphics and interactive techniques*, SIGGRAPH '93, pages 263–270. ACM, 1993.

[5] H. Carr, J. Snoeyink, and U. Axen. Computing contour trees in all dimensions. *Computational Geometry*, 24(2):75–94, 2003.

[6] H. Carr, J. Snoeyink, and M. van de Panne. Simplifying flexible isosurfaces using local geometric measures. *Proceedings of the conference on Visualization'04*, pages 497–504, 2004.

[7] R. Chan. *A Biofluid Dynamic Model for Centrifugal Accelerated Cell Culture Systems*. PhD Dissertation, Leipzig University, Germany, 2008.

[8] G. Chen, K. Mischaikow, R. S. Laramee, P. Pilarczyk, and E. Zhang. Vector field editing and periodic orbit extraction using morse decomposition. *Visualization and Computer Graphics, IEEE Transactions on*, 13(4):769–785, 2007.

[9] J. Ebling, A. Wiebel, C. Garth, and G. Scheuermann. Topology based flow analysis and superposition effects. In *Topology-based methods in visualization*, pages 91–103. Springer, 2007.

[10] R. Fuchs, J. Kemmler, B. Schindler, J. Waser, F. Sadlo, H. Hauser, and R. Peikert. Toward a Lagrangian vector field topology. In *Computer Graphics Forum*, volume 29, pages 1163–1172. Wiley Online Library, 2010.

[11] G. Haller. An objective definition of a vortex. *Journal of Fluid Mechanics*, 525:1–26, 2005.

[12] G. Haller and G. Yuan. Lagrangian coherent structures and mixing in two-dimensional turbulence. *Phys. D*, 147(3-4):352–370, Dec. 2000.

[13] H. Hauser, H. Hagen, and H. Theisel, editors. *Topology-based Methods in Visualization*. Mathematics and Visualization. Springer, 2007.

[14] C. Heine, D. Schneider, H. Carr, and G. Scheuermann. Drawing contour trees in the plane. *Visualization and Computer Graphics, IEEE Transactions on*, 17(11):1599–1611, 2011.

[15] J. Helman and L. Hesselink. Representation and display of vector field topology in fluid flow data sets. *Computer*, 22(8):27–36, Aug 1989.

[16] H. JCR, A. Wray, and P. Moin. Eddies, stream, and convergence zones in turbulent flows. *Center for turbulence research report CTR-S88*, pages 193–208, 1988.

[17] J. Jeong and F. Hussain. On the identification of a vortex. *Journal of fluid mechanics*, 285:69–94, 1995.

[18] J. Kasten, I. Hotz, B. R. Noack, and H.-C. Hege. On the extraction of long-living features in unsteady fluid flows. In V. Pascucci, X. Tricoche, H. Hagen, and J. Tierny, editors, *Topological Methods in Data Analysis and Visualization*, Mathematics and Visualization, pages 115–126. Springer Berlin Heidelberg, 2011.

[19] R. S. Laramee, H. Hauser, L. Zhao, and F. H. Post. Topology-Based Flow Visualization, The State of the Art. In *Topology-based Methods in Visualization*, pages 1–19, 2007.

[20] H. Li, W. Chen, and I.-F. Shen. Segmentation of discrete vector fields. *IEEE Transactions on Visualization and Computer Graphics*, 12(3):289–300, May 2006.

[21] I. Liu. *Continuum Mechanics*. Advanced Texts in Physics. Springer, 2002.

[22] S. E. Newhouse. *Lectures on dynamical systems*. Springer, 2011.

[23] A. Perry and M. Chong. A description of eddying motions and flow patterns using critical-point concepts. *Annual Review of Fluid Mechanics*, 19(1):125–155, 1987.

[24] A. Perry and M. Chong. Topology of flow patterns in vortex motions and turbulence. In *Eddy Structure Identification in Free Turbulent Shear Flows*, pages 339–361. Springer, 1993.

[25] A. Perry and D. Tan. Simple three-dimensional vortex motions in coflowing jets and wakes. *Journal of Fluid Mechanics*, 141:197–231, 1984.

[26] A. Pobitzer, R. Peikert, R. Fuchs, B. Schindler, A. Kuhn, H. Theisel, K. Matkovic, and H. Hauser. The State of the Art in Topology-based Visualization of Unsteady Flow. *Computer Graphics Forum*, 30(6):1789–1811, September 2011.

[27] H. Poincaré and R. Magini. Les méthodes nouvelles de la mécanique céleste. *Il Nuovo Cimento (1895-1900)*, 10(1):128–130, 1899.

[28] K. Polthier and E. Preu. Variational Approach to Vector Field Decomposition. In W. de Leeuw and R. van Liere, editors, *Data Visualization 2000*, Eurographics, pages 147–155. Springer Vienna, 2000.

[29] F. H. Post, B. Vrolijk, H. Hauser, R. S. Laramee, and H. Doleisch. The State of the Art in Flow Visualisation: Feature Extraction and Tracking. *Computer Graphics Forum*, 22(4):775–792, 2003.

[30] R. Serway and J. Jewett. *Principles of Physics: A Calculus-Based Text*. Number Bd. 1 in Available 2010 Titles Enhanced Web Assign Series. Cengage Learning, 2006.

[31] P. Skraba, B. Wang, G. Chen, P. Rosen, et al. 2D Vector Field Simplification Based on Robustness. In *Pacific Visualization Symposium (PacificVis), 2014 IEEE*, pages 49–56. IEEE, 2014.

[32] Y. Song. A note on galilean invariants in semi-relativistic electromagnetism. *arXiv preprint arXiv:1304.6804*, 2013.

[33] H. Theisel, T. Weinkauf, H.-C. Hege, and H.-P. Seidel. Topological methods for 2D time-dependent vector fields based on stream lines and path lines. *Visualization and Computer Graphics, IEEE Transactions on*, 11(4):383–394, July 2005.

[34] X. Tricoche. *Vector and Tensor Field Topology Simplification, Tracking and Visualization*. PhD thesis, University of Kaiserslautern, 2002.

[35] J. J. Van Wijk. Image based flow visualization. In *ACM Transactions on Graphics (TOG)*, volume 21, pages 745–754. ACM, 2002.

[36] T. Weinkauf, H. Theisel, K. Shi, H.-C. Hege, and H.-P. Seidel. Extracting Higher Order Critical Points and Topological Simplification of 3D Vector Fields. In *Proc. IEEE Visualization 2005*, pages 559–566, Minneapolis, U.S.A., October 2005.

[37] A. Wiebel, R. Chan, C. Wolf, A. Robitzki, A. Stevens, and G. Scheuermann. Topological flow structures in a mathematical model for rotation-mediated cell aggregation. In *Topological Methods in Data Analysis and Visualization*, pages 193–204. Springer, 2011.

[38] A. Wiebel, C. Garth, and G. Scheuermann. Localized Flow Analysis of 2D and 3D Vector Fields. In *EuroVis*, pages 143–150. Citeseer, 2005.

[39] E. Zhang, K. Mischaikow, and G. Turk. Vector field design on surfaces. *ACM Transactions on Graphics (TOG)*, 25(4):1294–1326, 2006.